Applied Catalysis B: Environmental 96 (2010) 338–349

Contents lists available at ScienceDirect

Applied Catalysis B: Environmental

journal homepage: www.elsevier.com/locate/apcatb

Preparation of $Ce_{0.67}Zr_{0.33}O_2$ mixed oxides as supports of improved Pd-only three-way catalysts

Bo Zhao[a,b], Guangfeng Li[a], Changhua Ge[b], Qiuyan Wang[a], Renxian Zhou[a,*]

[a] Institute of Catalysis, Zhejiang University, Hangzhou 310028, PR China
[b] School of Pharmaceutical and Chemical Engineering, Taizhou University, Taizhou 317000, PR China

ARTICLE INFO

Article history:
Received 4 September 2009
Received in revised form 19 February 2010
Accepted 23 February 2010
Available online 1 March 2010

Keywords:
CeO_2-ZrO_2 mixed oxides
Synthesis
Pd-only TWC
Stoichiometric windows

ABSTRACT

Four types of $Ce_{0.67}Zr_{0.33}O_2$ (CZCP, CZH, CZHP and CZM) mixed oxides as supports were prepared by coprecipitation, hydrothermal, homogeneous precipitation and microemulsion methods, respectively. The results show that both the preparation methods and the aging procedures have significant influences on the physicochemical properties of $Ce_{0.67}Zr_{0.33}O_2$ mixed oxides. All these fresh $Ce_{0.67}Zr_{0.33}O_2$ samples develop mesopore structure, especially that, CZCP obtains the largest diameter (20.87 nm) and volume (0.455 cm^3/g). The XRD results indicate that fresh CZHP and CZCP samples contain cubic and tetragonal phases, while only cubic solid solution is found in fresh CZH and CZM samples, which show better low-temperature reducibility. Moreover, higher oxygen storage capacity complete (OSCC) values and faster O_2 uptake are observed in CZH and CZM samples compared with those of fresh CZCP and CZHP. After calcination at 1100 °C, it is found that the OSCC values and the kinetics of the O_2 uptake for CZM and CZHP samples are deteriorated due to the coexistence of cubic and tetragonal phases as well as strong sintering of samples. On the contrary, the aged CZCP and CZH samples keep satisfactory low-temperature reducibility and oxygen storage capacity. For fresh catalysts, the pore-size distribution of mixed oxides seems to be important for catalytic activities. In contrast, for aged catalysts, their activities are related to both the redox properties and the textural properties of aged mixed oxides. Therefore, the Pd-only three-way catalyst supported on the CZCP exhibits the most promising amplified amplitude of stoichiometric window.

Crown © 2010 Published by Elsevier B.V. All rights reserved.

1. Introduction

The solid solution of ceria and zirconia-containing composite has attracted intensive interests for more than half a century for its far-ranging applications in catalytic processes [1–9]. Special attention has been paid to its crucial application as promoter of three-way catalyst (TWC), which is commonly used to reduce the emissions of CO, NO_x and hydrocarbons (HC) from automobile exhausts [1,10,11]. However, the high conversion efficiency of the TWC can only be achieved within a very narrow "operation window" of air to fuel ratio. In practice, the air to fuel ratio have to fluctuate around the theoretic value to some extent (typically 1 ± 0.05) due to the change of the operation modes of engine, resulting in that TWC cannot eliminate all three kinds of pollutants at the same time. It is, therefore, very essential and vital for an excellent TWC to have a large operation window even after repeated exposure to the actual auto-exhaust environment.

The addition of an oxygen storage agent into TWC is to enlarge the operation window and hence to achieve an optimal working efficiency under learn-burn and rich-burn conditions. CeO_2-based materials have been widely used as an oxygen storage material associated to the redox couple of Ce^{4+}/Ce^{3+}. The introduction of ZrO_2 into the ceria lattice significantly enhances the classical ceria behavior by its high thermal resistance, improved reduction efficiency, and excellent oxygen storage/release capacity [12–19]. Extensive studies have been made to explore the role of ceria and zirconia in the solid solution. It was found that the unique properties of the CeO_2-ZrO_2 solid solution result from the combination of oxygen storage capacity (OSC) of ceria and lattice defects and stabilization of ceria particles (preventing their thermal sintering) induced by zirconia [20–22].

However, the properties of these materials largely depend on the preparation methods [23–26]. Many preparation methods have been explored for the synthesis of CeO_2-ZrO_2 mixture oxide such as coprecipitation [14,27], hydrothermal synthesis [28], the polymerized complex method [29,30], high energy mechanical milling [1], sol–gel techniques [31], solution combustion [32], surfactant assistant approach [33], microemulsion [34] and some other techniques [35,36]. Almost the entire composition range with varying

* Corresponding author. Tel.: +86 571 88273290; fax: +86 571 88273283.
E-mail address: zhourenxian@zju.edu.cn (R. Zhou).

0926-3373/$ – see front matter. Crown © 2010 Published by Elsevier B.V. All rights reserved.
doi:10.1016/j.apcatb.2010.02.031

degrees of homogeneity and textual properties has been reported. Lamas et al. [37] reported a study of the tetragonal–cubic phase transition on nanocrystalline powders obtained by a pH controlled nitrate–glycine gel-combustion method. The characterization of CeO_2-ZrO_2 mixed oxides synthesized by two different chemical methods (citrate complexation and sol–gel) was reported by Alifanti et al. [38]. For low ceria contents, they reported that their sol–gel route gave rise to homogeneous solid solutions. However, an increase in ceria content (to >20%) led to a segregation of phases. Hori et al. [39] prepared CeO_2-ZrO_2 systems by coprecipitation, employing $(NH_4)_2Ce(NO_3)_6$ and $ZrO(NO_3)_2$ as cerium and zirconium precursors and calcination at 500 °C, which was claimed as the lowest temperature used so far to obtain CeO_2-ZrO_2 solid solution. These methods, however, are limited in their ability to produce CeO_2-ZrO_2 materials that retain high reducibility and OSC after extended treatments at temperatures in excess of 1000 °C.

Accordingly, due to the tendency to deactivate at high temperature for TWC there is a need for more thermally stable oxygen storage materials. Generally, Ce-rich compositions are preferred for the purposes of catalysis and better results are obtained based on $Ce_xZr_{1-x}O_2$ with x ranging from 0.6 to 0.8 [40]. In this study, aiming at improving the above-quoted properties, coprecipitation, homogeneous precipitation, microemulsion and hydrothermal methods were used to prepare $Ce_{0.67}Zr_{0.33}O_2$ mixed oxides. To the best of our knowledge, there is no open literature focusing on the investigation of the support preparation process and the stoichiometric window of the three-way catalysts simultaneously. Moreover, understanding these properties will provide important information to improve the performance of TWC for meeting more stringent emission regulations. In this paper, the catalytic performances of Pd-only TWC supported on different $Ce_{0.67}Zr_{0.33}O_2$ were studied. The textural and redox properties of the supports were revealed. Moreover, the relations between properties of the support and the catalytic performances of TWC had also been investigated.

2. Experimental

2.1. Synthesis of $Ce_{0.67}Zr_{0.33}O_2$

2.1.1. Coprecipitation method

The nitrates $Ce(NO_3)_3$ and $ZrO(NO_3)_2$ were mixed under continuous stirring. The molar ratio of Ce:Zr was 67:33. The solution of aqueous NH_3 was dropped into the mixed salt solution under continuous stirring and the pH value was controlled to be 9.5. After aging at room temperature for 12 h, the precipitate was filtered and washed with deionized water until no pH change could be detected [27]. Then the precipitate was dried under supercritical condition in alcohol (250 °C, 7.5 MPa) for 3 h.

2.1.2. Homogeneous precipitation method

Urea was added to the quantitative mixed solution of $Ce(NO_3)_3$ and $ZrO(NO_3)_2$ under continuous stirring condition and the molar ratio of urea: (Ce + Zr) was 17. Then, the mixture was transferred to a hot oil bath and heated at 100 °C with vigorous stirring for 3 h. The resulting suspension was then cooled to room temperature and aged at room temperature for 12 h before the solid precipitate was filtered and washed with deionized water. Finally, the precipitate was dried at 110 °C for 2 h [41].

2.1.3. Microemulsion method

In this preparation procedure, a microemulsion containing cerium and zirconium nitrate was prepared as follows. First, cetyltrimethylammonium bromide (CTAB) was mixed with butanol and cyclohexane with stirring until the mixture became transparent and the molar ratio of [CTAB]:[butanol]:[cyclohexane] was 1:8:34. Then, 9.5 ml of the mixed solution of $Ce(NO_3)_3$ and $ZrO(NO_3)_2$ with desired Ce:Zr ratio was added into the mixture under vigorous agitation. Another microemulsion containing the solution of aqueous ammonia was also prepared under the same procedure described above. Then, the microemulsion containing cerium and zirconium nitrate solution was mixed with the other one containing aqueous ammonia. The reaction mixture was stirred until the solution was suspended by formed colloidal particles. After aging at room temperature for 24 h, the precipitate was filtered, washed with deionized water and dried at 110 °C for 2 h [42,43].

2.1.4. Hydrothermal method

The solution of aqueous ammonia was added to the mixed ethanol solution of $Ce(NO_3)_3$, $ZrO(NO_3)_2$ and CTAB under vigorous agitation. The molar ratio of Ce:Zr was 67:33 and (Ce + Zr)/CTAB was kept at 1.0. The pH value of the mixture was adjusted to 9.5. Then the slurry was sealed in a Teflon-lined stainless autoclave and hydrothermally treated at 100 °C for 1 h. The precipitate was separated by filtration, washed with deionized water until no pH change could be detected, and dried at 110 °C for 2 h [44].

Finally, all these four samples were calcined at 500 °C for 4 h in air and denoted as fresh samples of CZCP, CZHP, CZM and CZH, respectively. In addition, the mixed oxides were further calcined at 1100 °C for 4 h in dry air to obtain aged samples during the investigation of thermal stability.

2.2. Catalyst preparation

The Pd-only three-way catalysts with different supports were prepared by incipient impregnation method with aqueous solutions of H_2PdCl_4 as metal precursors (Sinopharm Chemical Reagent Co., Ltd.). Pd loading was 0.5 wt%. The impregnated samples were reduced with hydrazine hydrate, and washed with a large amount of deionized water until no Cl^- ions was detected in the filtered solution. The catalysts were dried at 110 °C and then calcined at 500 °C for 2 h. These as-prepared fresh catalysts were denoted as Pd/CZCP, Pd/CZHP, Pd/CZM and Pd/CZH, respectively. In order to compare their thermal stability, the catalysts were further submitted to aging at 1100 °C for 4 h in dry air, which were denoted as Pd/CZCP-a, Pd/CZHP-a, Pd/CZM-a and Pd/CZH-a, respectively.

2.3. Physicochemical characterization

BET surface area, pore volume and pore-size distribution of ceria–zirconia mixed oxides were measured by N_2 adsorption using an OMNISORP 100CX apparatus. Prior to adsorption measurements, samples were degassed at 200 °C for 2 h under vacuum. Then N_2 adsorption was carried out at the liquid nitrogen temperature.

The powder X-ray diffraction (XRD) experiment was recorded on a Rigaku D/Max-IIIB diffractometer employing monochromatic Cu Kα radiation. The X-ray tube was operated at 40 kV and 40 mA. The X-ray powder diffractogram was recorded at 0.02° intervals in the range of $20° \leq 2\theta \leq 80°$.

The X-ray photoelectron spectroscopy (XPS) experiments were carried out on a PHI-Quantera SXM system equipped with a monochromatic Al Kα X-rays under ultra-high vacuum (6.7×10^{-8} Pa). Sample charging during the measurement was compensated by an electron flood gun. The XPS data from the regions related to the C 1s, O 1s, Zr 3d, Ce 3d and Pd 3d core levels were recorded for each sample. The binding energies were calibrated internally by the carbon deposit C 1s binding energy (BE) at 284.8 eV. The deconvolution method of XPS spectra is fitted by Gaussian function.

Hydrogen-temperature-programmed reduction (H_2-TPR) experiment was carried out in a flow system to observe the reducibility of the mixed oxides. Typically 0.05 g of sample was

employed. The standard pretreatment consisted of heating the sample in air from room temperature to 300 °C, holding at that temperature for 30 min, and cooling down to 150 °C in air. Then the sample was further purged in flowing He (40 ml min^{-1}) for 1 h. After that, the sample was heated under flowing H_2 (5% in Ar, 40 ml min^{-1}) at a rate of 10 °C min^{-1} to 900 °C. The outlet gases were analyzed on-line by a gas chromatograph (GC, KX100) with a TCD, and the effluent H_2O formed during H_2-TPR was adsorbed with a 5 A molecular sieve.

UV-Raman spectra were recorded on a UV-HR Raman spectrograph with He-Gd laser of 325 nm excitation wavelength. The spectral resolution was 4 cm^{-1}, and the spectra acquisition consisted of 2 accumulations of 30 s for each sample. A frequency range of 100–1000 cm^{-1} was observed.

Oxygen storage capacity (OSC) of prepared ceria–zirconia mixed oxide was measured by pulse injection technique. The amount of oxygen consumed during the reoxidation stage was referred to as oxygen storage capacity complete (OSCC) and the experiments were performed with a CHEMBET-3000 (Quantachrome Instrument Co. Ltd., American) as the analytical device. The samples were first reduced in the H_2 flow (10 ml min^{-1}) from room temperature to 550 °C at a rate of 10 °C $min^{-1}$and maintained at 550 °C for 60 min. After that, the samples were cooled to 400 °C in H_2 flow and purged with He for 30 min. An oxygen pulse was injected every 5 min to the samples in the main stream of He (30 ml min^{-1}) to obtain the breakthrough curve, from which the OSCC was determined.

The size of the metallic particles on the supported Pd catalysts was checked with transmission electron microscopy using a JEM-2010 (HR) apparatus operated at 200 kV.

2.4. Catalytic activity test

The three-way catalytic activity was evaluated in the fixed-bed reactor with the simulated exhaust gas containing NO (1000 ppm), NO_2 (300 ppm), C_3H_6 (670 ppm), C_3H_8 (330 ppm), CO (7500 ppm), O_2 and Ar (balance) and their flow rates were controlled by mass flow controllers before entering the blender [45]. The concentration of CO, NO_x (NO and NO_2) and total HC (C_3H_6 and C_3H_8) were analyzed by a Bruker EQ55 FTIR spectrometer coupled with a multiple reflection transmission cell (Infrared Analysis Inc). The space velocity was 43,000 h^{-1} and 0.2 ml of catalysts (40–60 mesh) were loaded in the reactor. The air/fuel ratio experiments were carried out at 400 °C. The concentration of O_2 was adjusted in the tests of air/fuel ratio from 850 ppm to 8440 ppm. The S value of the simulated exhaust, which represents the ratio between the available oxygen and the oxygen needed for full conversion to CO_2, H_2O and N_2, is defined as $S = \{2[O_2] + [NO] + 2[NO_2]\}/\{9[HC] + [CO]\}$, $S = 1$ was at stoichiometry and the corresponding concentration of O_2 was 7450 ppm [46].

3. Results and discussion

3.1. XRD characterization

The X-ray diffraction patterns of four types of $Ce_{0.67}Zr_{0.33}O_2$ samples are shown in Fig. 1. The major peaks of the XRD patterns of all samples are consistent with the characteristic peaks of cubic CeO_2, which indicate the formation of CeO_2-ZrO_2 solid solutions. The average lattice constants of these CeO_2-ZrO_2 materials are calculated based on the Bragg's Law ($2d \sin\theta = k\lambda$) with the four major peaks corresponding to the (1 1 1), (2 0 0), (2 2 0) and (3 1 1) crystallographic planes. For the fresh samples as shown in Fig. 1, CZH and CZM only present the cubic peaks ascribed to a fluorite lattice structure pattern and the lattice constant is 0.53891 and 0.53552 nm,

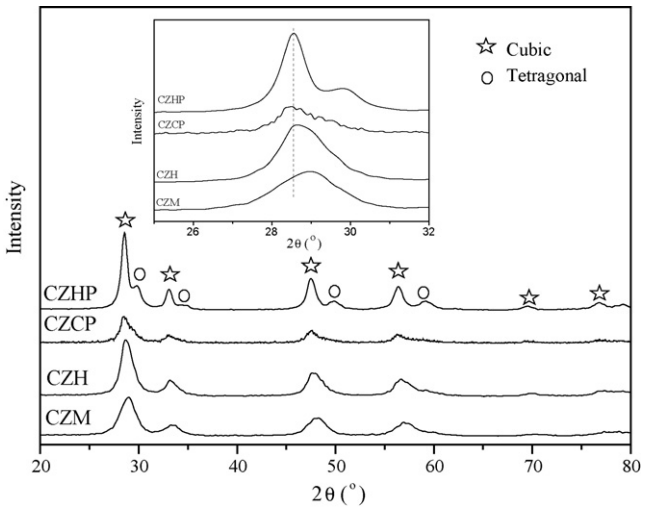

Fig. 1. XRD patterns of fresh $Ce_{0.67}Zr_{0.33}O_2$ samples prepared by different methods.

respectively. No extra peaks attributed to non-incorporated ZrO_2 are observed in XRD patterns of CZH and CZM. These results indicate that Ce and Zr ions are homogeneously distributed in the as-prepared powders and $Ce_{0.67}Zr_{0.33}O_2$ solid solutions with cubic fluorite structure are formed for CZH and CZM. Meanwhile, for the fresh CZHP and CZCP samples, distinguishable separated peaks and asymmetric peaks are observed respectively, suggesting the presence of two phases. The minor peaks of tetragonal Zr-rich phase, whose composition is approximately $Ce_{0.1}Zr_{0.9}O_2$ for CZHP and $Ce_{0.12}Zr_{0.88}O_2$ for CZCP, are found in the corresponding XRD patterns. The major phase is a cubic solid solution of CeO_2-ZrO_2 with the lattice constant of 0.54084 and 0.54070 nm for CZHP and CZCP, respectively, which is smaller than the theoretical value of 0.541 nm for ceria. Since the ionic radius of Zr^{4+} (0.084 nm) is smaller than that of Ce^{4+} (0.097 nm) for eight-coordination [12], the lattice constant of the cubic cell of CeO_2-ZrO_2 declines with the increase of the Zr^{4+} in the mixed oxides. In contrast, CZM and CZH samples show much larger shifts in peak position (Fig. 1 inset), corresponding to the smaller cell parameters compared with those of CZCP and CZHP samples. Based on the variations of the value of the lattice constant, it is hereby entirely reasonable to speculate that more Zr^{4+} ions have entered into the ceria lattice and atomically more homogeneous mixed oxides have formed in CZM and CZH compared with CZCP and CZHP. Thus it can be concluded, to a great extent, the crystal structure of CeO_2-ZrO_2 mixed oxides are determined by preparation methods. It appears difficult to form homogenous mixed oxides for the precipitated precursors such as in the case of the coprecipitation and homogeneous precipitation. Since the rates of precipitation between the two metals are quite different [12,47], it may be difficult to simultaneously precipitate both Ce and Zr salts without appropriate chemical modifications of the precipitation process. However, the microemulsion method is considered to be a suitable method leading to high degree of homogeneity of the mixed oxides product [48]. The preparation of the gel precursor using organic agent and CTAB leads to a homogeneous dispersion at molecular level of the Ce and Zr species, which then upon calcination leads to adequate mixed oxides. The suspension obtained by hydrothermal method contributes a similar effect as well.

As shown in Fig. 2, after aging treatment, all samples show narrower diffraction lines, which indicate the larger crystallites. A visible Zr-rich phase can be identified in the XRD patterns of all samples after calcination at 1100 °C, especially for CZHP. The lattice constant of the major cubic phase increases to 0.54094 nm for the aged CZHP due to segregation of more Zr species [49], which is confirmed by the clear existence of tetragonal phase. On the other

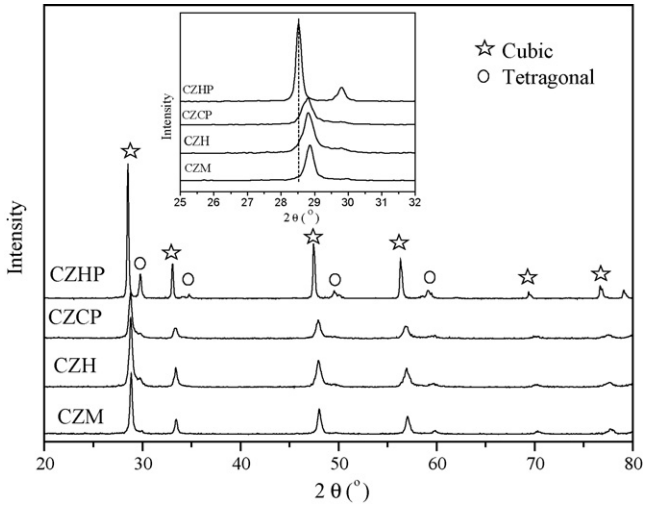

Fig. 2. XRD patterns of aged $Ce_{0.67}Zr_{0.33}O_2$ samples prepared by different methods.

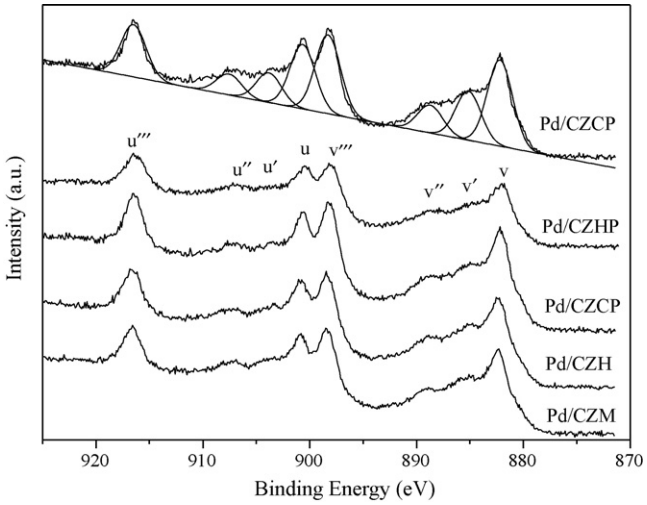

Fig. 3. Ce 3d XPS spectra for the fresh catalysts based on different supports.

hand, for the aged CZCP, CZH and CZM, the lattice constant of the major cubic phase decreases obviously to 0.53647, 0.53609 and 0.53506 nm, respectively. It can be confirmed from the XPS results in the following discussion (Table 1) that the concentrations of oxygen vacancies and Ce^{3+} ions decrease with increasing crystallite size after ageing. As a result, more Ce^{3+} (0.114 nm) transforming to Ce^{4+} (0.097 nm) induces the shrinkage of lattice parameters [50]. It should be noticed that the lowest 2θ value of CeO_2 (1 1 1) diffraction peak is observed (Fig. 2 inset) for the CZHP sample due to its biggest lattice constant.

The average particle sizes of $Ce_{0.67}Zr_{0.33}O_2$ samples are determined by the Scherrer equation. For fresh samples, the particle size increases in the order of CZM (4.2 nm) < CZH (5.3 nm) < CZCP (7.9 nm) < CZHP (10.4 nm). After aging, the particle size for CZM, CZH, CZCP and CZHP is 33.1, 22.3, 21.4 and 86.3 nm, respectively. The increasing amplitude of particle size follows a sequence of CZHP (730%) > CZM (688%) > CZH (321%) > CZCP (171%). For aged samples, it can be seen that the smallest particle size is achieved by the sample prepared by coprecipitation method.

On the basis of these results it can be concluded that the crystal structure of $Ce_{0.67}Zr_{0.33}O_2$ mixed oxides and their thermal stability are determined by preparation methods. The mixed oxide prepared by coprecipitation shows well thermal stability, which may be related to the supercritical-drying method.

3.2. XPS studies

XPS investigation was conducted to provide information of the surface elemental distribution and the oxidation states of cerium. As presented in Fig. 3, the curves of Ce 3d spectra are composed of eight peaks corresponding to four pairs of spin–orbit doublets.

Table 1
Surface elemental composition and oxidation state of Ce measure by XPS.

Sample	Surface composition (at.%)				Ce/Zr ratio	Ce^{3+} in Ce (%)
	Ce 3d	Zr 3d	Pd 3d	O 1s		
Pd/CZCP	21.00	9.35	0.01	69.64	2.25	19.26
Pd/CZHP	20.83	6.95	0.03	72.19	3.0	17.69
Pd/CZH	18.85	7.94	0.05	73.16	2.37	19.37
Pd/CZM	19.78	7.62	0.05	72.55	2.60	19.65
Pd/CZCP-a	18.46	10.17	0.13	71.24	1.82	18.53
Pd/CZHP-a	21.05	7.65	0.28	71.02	2.75	17.56
Pd/CZH-a	19.31	9.10	0.13	71.45	2.12	18.69
Pd/CZM-a	18.85	7.74	0.22	73.19	2.44	17.43

The labeling of the peaks follows the convention [51,52]. Letters u and v refer to the $3d_{3/2}$ and $3d_{5/2}$ spin–orbit components, respectively. The spin–orbit splitting, in accordance with the literatures [53], is 18.4 eV. The peaks marked as u (900.6–901.0 eV), u″ (907.5–907.7 eV) and u‴ (916.6–916.9 eV) arise from Ce^{4+} $3d_{3/2}$ while the peaks labeled as v (882.2-882.6 eV), v″ (889.1–889.3 eV) and v‴ (898.2–898.5 eV) arise from Ce^{4+} $3d_{5/2}$. The couples corresponding to one of the two possible electron configuration of the final state of the Ce^{3+} species are labeled as u′ (903.5–904.2 eV) and v′ (885.1–885.8 eV). The proportion of Ce^{3+} cation with regard to the total cerium is calculated from the ratio of the sum of areas of the Ce^{3+} species to the sum of areas of the total cerium species. The surface elemental contents calculated from the normalized peak areas of Ce 3d, Zr 3d, Pd 3d and O 1s core level spectra are listed in Table 1. Using the values of surface atomic composition in Table 1, an estimation of the Ce/Zr can be obtained for the depth probed by XPS. The surface Ce/Zr atomic ratio of all fresh samples is higher than the theoretical atomic ratio of 2.0, which means the outer part is rich in the cubic Ce-rich phase. On the other hand, the migration of Zr from the bulk to the surface during aging process can be indicated by the decrease of Ce/Zr ratio. A similar result has been reported by Fan et al. [54]. The gaps between the Ce/Zr ratios of fresh and aged samples are the result of the reorganization of phases with different Zr composition, forming a so-called "shell-core" structure with the high-Zr-composition phase in the outer sphere of the particles [54]. The surface content of Pd element increases significantly after aging for all catalysts. Probably the main reason for this is the variation in specific surface area, since the area density of Pd on the support surface must increase as the oxide support undergoes sintering [55]. However, in the cases of Pd/CZHP-a and Pd/CZM-a catalysts, the surface concentration of Pd species increases more significantly compared with those of Pd/CZCP-a and Pd/CZH-a, which suggests the sintering of Pd on the surface due to the weak interaction between Pd species and these two supports during the thermal aging process [56].

Table 1 also lists the relative concentration of Ce^{3+} in Ce. By quantifying the surface Ce^{3+} ions according to curve-fitted data, it is found that the concentration of Ce^{3+} ions decreases in the order of Pd/CZM > Pd/CZH > Pd/CZCP > Pd/CZHP. As reported in literature [53] and the references therein, the presence of Ce^{3+} is associated with the formation of oxygen vacancies. Therefore, the formation of homogeneous CZ solid solution seems to facilitate the reduction of Ce^{4+} to Ce^{3+} or oxygen vacancy formation. During aging treatment, the decrease of the Ce^{3+} content can be seen, which

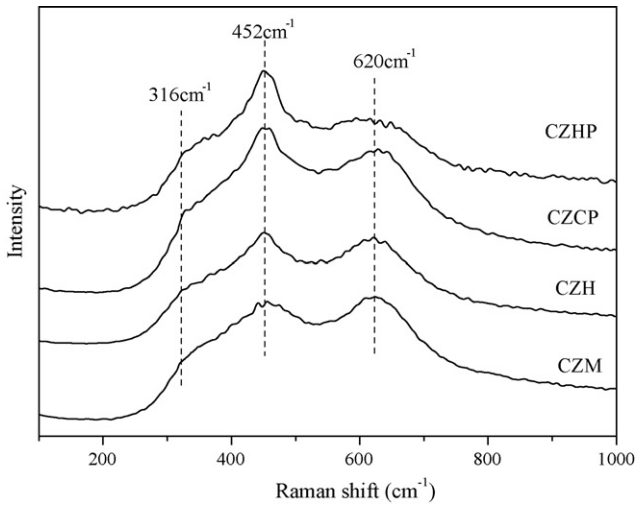

Fig. 4. UV-Raman profiles of fresh $Ce_{0.67}Zr_{0.33}O_2$ samples prepared by different methods.

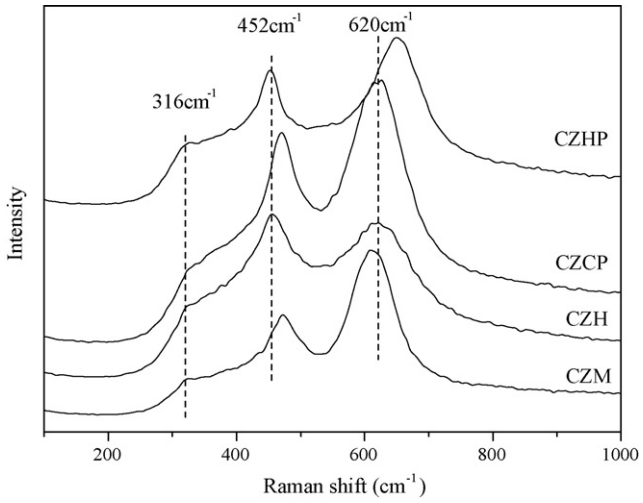

Fig. 5. UV-Raman profiles of aged $Ce_{0.67}Zr_{0.33}O_2$ samples prepared by different methods.

is likely due to the reduction of noble metal by the cerium component and/or the aging treatment in air [57]. As for the aged catalysts, the concentration of Ce^{3+} follows the sequence of Pd/CZH-a > Pd/CZCP-a > Pd/CZHP-a > Pd/CZM-a, which suggests that more oxygen vacancies preserve for the aged CZ sample prepared by hydrothermal and coprecipitation methods than those by homogeneous precipitation and microemulsion method.

3.3. Raman characterization

In contrast to XRD results, which yield information related to the cation sublattice, Raman spectroscopy of these oxide structures is dominated by oxygen lattice vibrations. It is sensitive to the crystal symmetry, thus being a potential tool to obtain additional structural information.

Fig. 4 shows the comparison of Raman spectra of fresh $Ce_{0.67}Zr_{0.33}O_2$ samples prepared by different methods. It can be seen that two obvious bands at 452 and 620 cm^{-1} are observed. The band at around 452 cm^{-1} is attributed to the single Raman active mode of F_{2g} symmetry allowed for the fluorite structure [31,58]. The bands at about 620 cm^{-1} can be linked to oxygen vacancies in the CeO_2 lattice and attribute to the presence of defective structure in CeO_2-ZrO_2 materials [59]. The intensity ratio between the peak at 620 cm^{-1} and the peak at 452 cm^{-1} is 0.96, 0.88, 0.79 and 0.55 for CZM, CZH, CZCP and CZHP, respectively. The ratio follows the sequence of CZM > CZH > CZCP > CZHP, which indicates that the amount of defects in $Ce_{0.67}Zr_{0.33}O_2$ samples is strongly affected by the preparation methods. The samples prepared by microemulsion and hydrothermal methods have more oxygen vacancies compared with those prepared by coprecipitation and homogeneous precipitation methods. The appearance of weak band at about 316 cm^{-1} can be attributed to the displacement of oxygen atoms from their ideal fluorite lattice positions [16,59]. Such a spectral feature is attributed to the presence of a t″ phase, where cation sublattice remains cubic structure while oxygen atoms undergo a tetragonal distortion [60]. The metastable t″ cannot be effectively detected by XRD technique due to weak diffraction ability of oxygen atoms, but be distinguished by the Raman spectroscopy thanks to its higher sensitivity to the oxygen displacements and smaller detection domain [50].

Fig. 5 shows the Raman spectra of the $Ce_{0.67}Zr_{0.33}O_2$ samples calcined at 1100 °C.

It is important to note that the intensities of the F_{2g} band are stronger than those of fresh ones. It should be mentioned here that the intensity of the Raman band depends on several factors including grain size and morphology. Therefore, it is quite obvious that sintering of the samples at high calcination temperatures increases the intensity of the F_{2g} band, which is in agreement with XRD measurements [61,62]. In particular, the obvious shift of the band at 452 cm^{-1} to higher wave number is observed in the aged CZCP, which could be due to the evident increase in the zirconium content in the ceria–zirconia solution after aging as evidenced by XPS results [61]. As for the aged CZM sample, the obvious upshifted band of 452 cm^{-1} is related to the CeO_2-ZrO_2 solid solution as a consequence of the minimum lattice parameter among all aged samples brought about by oxidation of Ce^{3+} to Ce^{4+} during aging [27]. On the other hand, the obvious shift of the band at 620 cm^{-1} is observed in the aged CZHP, which is ascribed to the overlapping of another peak at 646 cm^{-1}, indicating a typical tetragonal structure. These results are in good agreement with the XRD characterization and the obvious presence of the tetragonal Zr-rich solid solution has been observed in the aged CZHP.

Table 2
Textural property of $Ce_{0.67}Zr_{0.33}O_2$ samples prepared by different methods.

Sample	Calcination temperature (°C)	Surface area (m^2/g)	Mesopore volume (cm^3/g)	Mesopore diameter (nm)	Micropore volume (cm^3/g)	Micropore diameter (nm)
CZCP	500	122.0	0.455	20.87	0.039	1.19
CZHP	500	82.6	0.103	13.88	0.025	1.22
CZH	500	89.0	0.156	12.62	0.025	1.24
CZM	500	127.6	0.166	8.22	0.039	1.19
CZCP	1100	5.4	0.041	33.40	–	–
CZHP	1100	3.1	0.011	38.78	–	–
CZH	1100	7.2	0.062	35.92	–	–
CZM	1100	2.6	0.0017	40.68	–	–

Aged in dry air at 1100 °C.

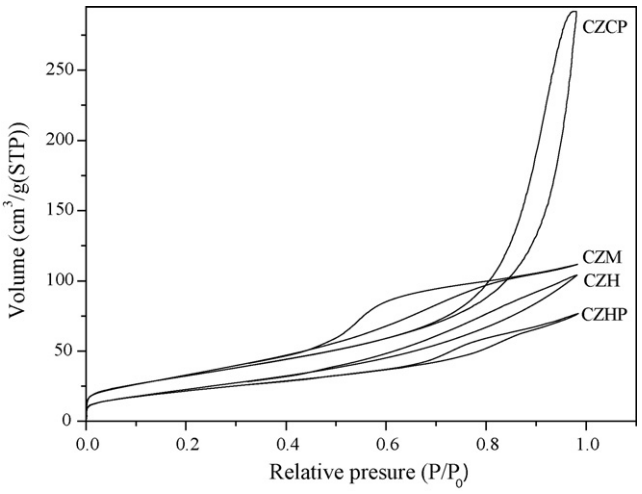

Fig. 6. Nitrogen adsorption/desorption isotherms of fresh $Ce_{0.67}Zr_{0.33}O_2$ samples prepared by different methods.

3.4. Textural properties

Table 2 lists the BET surface areas of $Ce_{0.67}Zr_{0.33}O_2$ prepared by different methods. Generally speaking, the BET surface area is mainly determined by the preparation procedures of materials. Low calcination temperature, such as 500 °C in this case, often leads to a sample with high-surface area. As listed in Table 2, the specific surface areas of the fresh samples are in the order of CZM > CZCP > CZH > CZHP, which are all higher than 80 m^2/g. It is noted that the surface area of CZM is extremely large due to the microemulsion precursor formed in the water/oil system [12] and that of CZCP takes second place due to the supercritical-drying method. The micropore properties of the fresh samples are similar. Nitrogen adsorption/desorption isotherms and the pore-size distribution of all fresh $Ce_{0.67}Zr_{0.33}O_2$ samples are shown in Figs. 6 and 7, respectively. The isotherms (Fig. 6) are identified as type IV and H_2 hysteresis, characteristic of mesoporous material. From Fig. 7 we can see that the pore-size distribution for CZHP, CZH and CZM is not uniform and the average pore size is small. Especially for CZM and CZH, the average mesopore diameter is 8.22 and 12.62 nm, respectively. However, we can see that the pore-size distribution is uniform for CZCP and the maximum of pore distribution is observed at around 20.87 nm, which indicates that the pores might consist of the voids among original particles. Meanwhile, an interesting observation is that the mesopore volume of $Ce_{0.67}Zr_{0.33}O_2$ prepared by coprecipitation is 0.455 cm^3/g, which is significantly larger than others. The textural properties such as surface area, pore volume and average pore diameter, play an important role in the performance of catalytic supports, especially for the catalytic supports used in high space velocity, which requires the supports to have larger surface area, pore volume and good pore diameter distribution [63]. As a result, CZCP sample should be more suitable as catalytic carrier and can be employed in high space velocity conditions.

It is also worth noting that no micropores exist for all oxide samples after calcination at 1100 °C. Furthermore, the surface area and pore volume of all oxide samples are found to decrease drastically together with increasing of mesopore diameter. The surface area of CZCP, CZHP, CZH and CZM is 5.4, 3.1, 7.2 and 2.6 m^2/g, respectively. The decrease in the surface area and pore volume is a common phenomenon due to sintering of the samples at high temperature. In addition, the surface areas of the aged samples decrease in the order of CZH > CZCP > CZHP> CZM, which indicates that the mixed oxides prepared by hydrothermal and coprecipitation have better texture stabilities than those prepared by homogeneous precipitation and microemulsion.

3.5. H_2-TPR studies

The results of temperature-programmed reduction (TPR) of $Ce_{0.67}Zr_{0.33}O_2$ mixed oxides before and after aging are shown in Fig. 8. As shown in Fig. 8(a), a peak appears at 800 °C in the TPR profile of the fresh CZHP, which is ascribed to the reduction of the bulk oxygen and is usually observed over ceria [12]. In agreement with the XRD observation, the separation of Ce-rich and Zr-rich phases occurs upon calcination at 500 °C after the homogeneous precipitation process. However, for fresh CZCP and CZH samples, the reduction temperature of the bulk oxygen decreases from 800 to 765 °C, indicating the increase of bulk oxygen mobility, thus improving the reducibility of bulk oxygen. On the contrary, for fresh CZM sample, no high temperature reduction peak is found. We suggest that there are two possible reasons: (i) According to XRD and BET results, CZM sample presents the smallest crystal size and the highest surface area, therefore most of the oxygen locates on surface. (ii) The bulk oxygen mobility has been greatly enhanced due

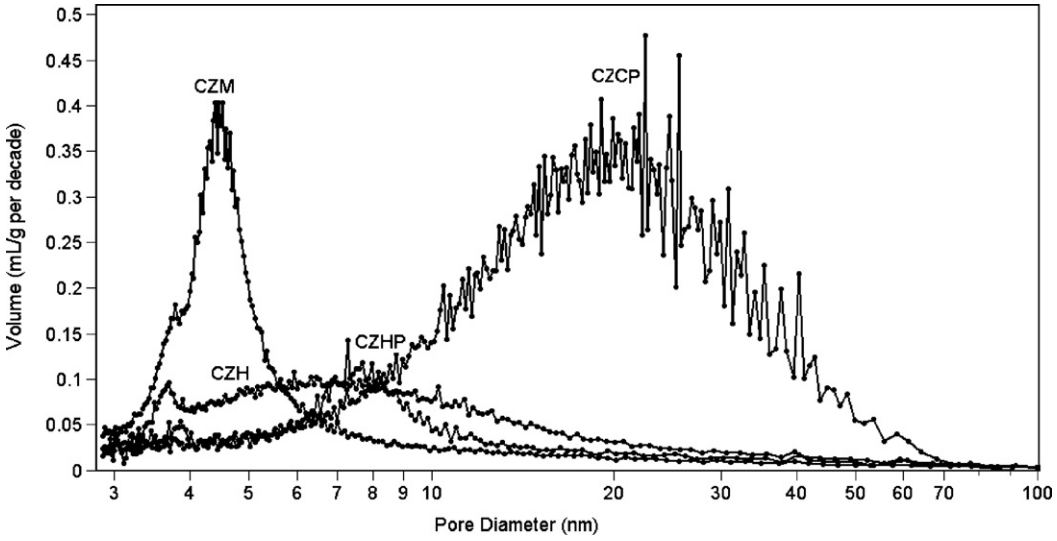

Fig. 7. Pore-size distribution of CZ samples prepared by different methods.

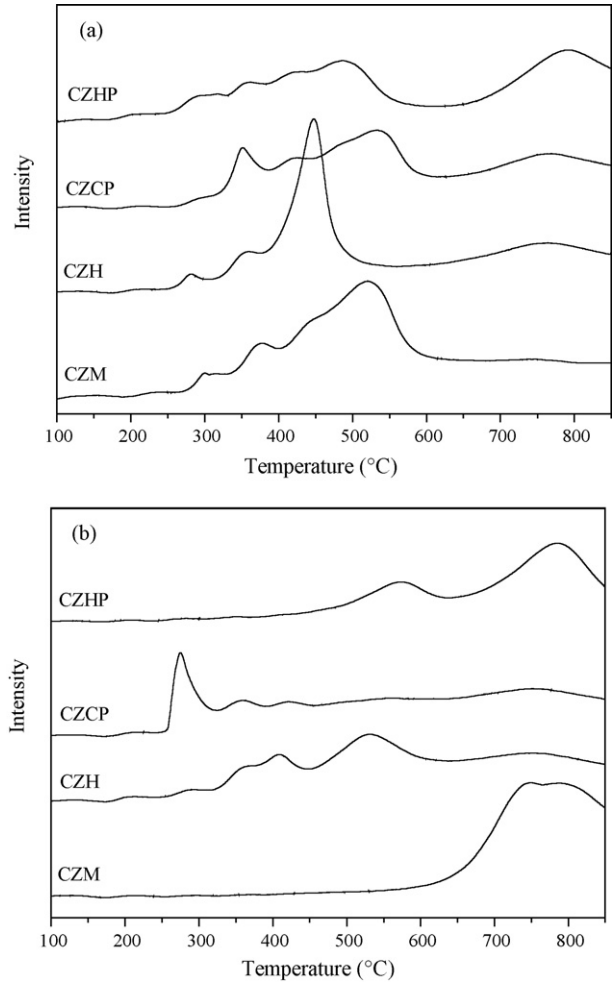

Fig. 8. H_2-TPR profiles of the fresh (a) and aged (b) $Ce_{0.67}Zr_{0.33}O_2$ samples prepared by different methods.

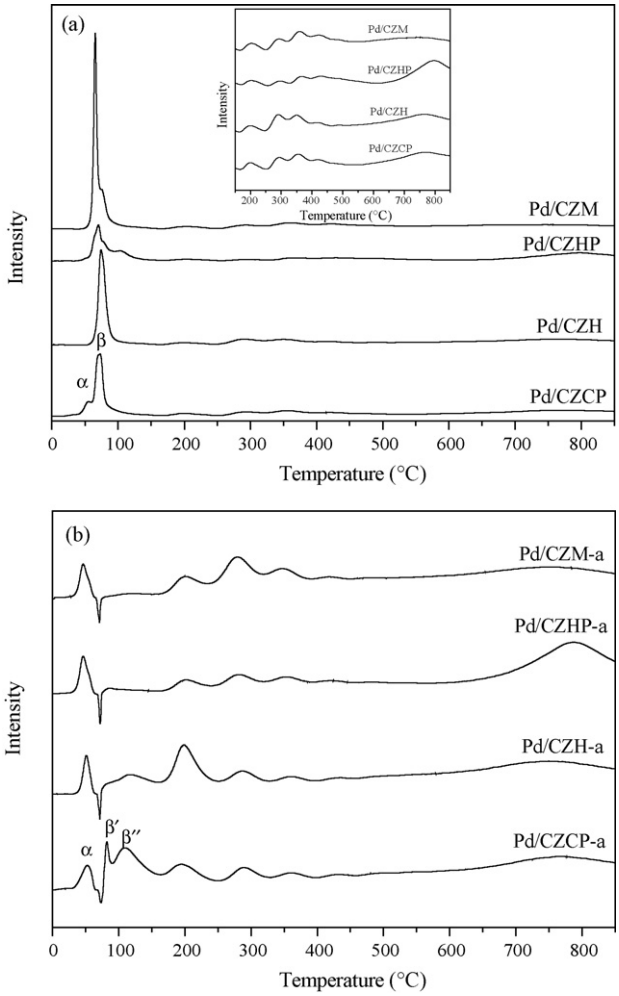

Fig. 9. TPR profiles of different catalysts calcined at (a) 500 °C and (b) 1100 °C.

to the high homogeneity and the amount of defects. Consequently, the bulk oxygen can move to surface or subsurface more easily during the reduction process. The low-temperature reducibility (below 600 °C) of the fresh $Ce_{0.67}Zr_{0.33}O_2$ is typically characterized by the presence of more than one peak which is somehow overlapped. Its multimodal shape can be attributed to the reduction of oxygen species adsorbed on the oxygen vacancies which are generated by the formation of the solid solutions [62], the reduction of surface Ce^{4+} of the mixed oxide crystallites and the reduction with subsurface oxygen supplied from the bulk [12,17,31,64]. The reduction peaks below 600 °C are more prominent and shift to lower temperatures for CZM and CZH samples compared to those of CZCP and CZHP. Moreover, CZCP hardly shows large amount of H_2 consumption in the low-temperature region, although it has the similar BET surface area compared to that of CZM. As discussed in the XRD analysis, fresh CZM and CZH samples exhibit more homogeneous solid solution, but fresh CZCP and CZHP samples present cubic and tetragonal phases. Thus, it is proposed that the reducibility can be modified remarkably by enhancing the homogeneity of $Ce_{0.67}Zr_{0.33}O_2$ mixed oxides.

Significant changes in reducibility happen for CZM and CZHP samples after aging treatment in Fig. 8(b). For example, the reduction of surface oxygen disappears for CZM due to the remarkably reduced surface area after aging, while the reduction of bulk oxygen at high temperature emerges. As for the aged CZHP sample, the low-temperature oxygen reduction exhibits only one peak and its peak temperature is retarded up to 573 °C, which may be resulted from the reduced surface area. Based on the above discussions, we can conclude that the reducibility of CZM and CZHP is obviously deteriorated after aging treatment. However, the aged CZCP and CZH still exhibit low-temperature reducibility due to the relatively high-surface area. Moreover, for the aged CZCP, the first low-temperature reduction peak shifts from 293 to 277 °C, which could be attributed to the most increase in the zirconium content in the ceria–zirconia solution as evidenced by XPS results and the modifications of the oxygen sublattice after aging. The shift of the reduction peak indicates that the coprecipitation method in our research can provide the $Ce_{0.67}Zr_{0.33}O_2$ mixed oxides with better reduction properties especially after aging treatment. Furthermore, from Fig. 8(b) we can also see that the intensity of reduction peak of bulk oxygen decreases for aged CZCP and CZH compared with that of aged CZHP and CZM samples, indicating that for the former two samples the bulk oxygen mobility has improved despite surface sintering of these samples during aging treatment.

H_2-TPR profiles of the Pd-supported catalysts are shown in Fig. 9. We can see that H_2-TPR profiles of fresh catalysts below 150 °C exhibit two hydrogen consumption peaks. According to the previous work in our research group, the TPR profile for Pd/Ce-Zr-O catalyst shows that the PdO species is reduced at 60–90 °C [65]. Thus, we suggest that the α peak is attributed to the reduction of highly dispersed PdO species and the β peak is ascribed to the reduction of stable PdO species having strong interaction with support. However, according to calculation, the total amount of the H_2 consumption of peak β is too large to be reasonably attributed to

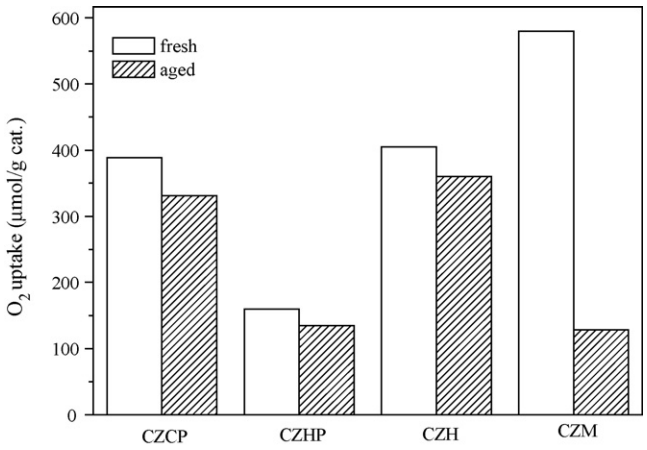

Fig. 10. OSCC values at 400 °C of $Ce_{0.67}Zr_{0.33}O_2$ samples prepared by different methods.

the reduction of noble metal oxides, as the amount of noble metal loaded is far too small (0.5 wt%). It is well known that the oxidation of H_2 on the precious metal catalysts relies heavily on the spillover effect, which splits H_2 molecules into H atoms by precious metal. These highly reactive H atoms can easily reduce oxides by donating electrons at relatively low temperature [53]. Therefore, we suggest that the presence of palladium facilitates the adsorption and spillover of hydrogen from the noble metal particles to the support, resulting in the interfacial Ce^{4+} reduction at low temperature [53,55]. Moreover, the first reduction-peak temperature is 53, 75, 71 and 66 °C for Pd/CZCP, Pd/CZH, Pd/CZHP and Pd/CZM, respectively, and Pd/CZCP catalyst exhibits the best reduction capacity. In addition, the reduction peaks above 150 °C ascribed to surface and bulk oxygen of CZ are still evident, but shift to lower temperature in comparison with that of the pure support (Fig. 8(a)), which can be attributed to the presence of Pd promotes the reduction of CZ via the spilling of hydrogen [45]. In contrast, the intensity of reduction peak at low-temperature region is weakened for aged catalysts in Fig. 9(b), implying that Pd was partly sintered after aging [66]. Furthermore, after aging treatment significant changes in the reduction characteristics happen for all catalysts. A new negative peak can be observed at about 70 °C, which is generally attributed to the decomposition of palladium hydride [65]. It is worth noting that splitting of peak β is observed in the Pd/CZCP-a and Pd/CZH-a catalysts. Peak β′ is ascribed to the reduction of stable PdO species having strong interaction with support and peak β″ is related to the reduction of Ce^{4+} located at the interface of palladium species. On the contrary, peak β disappears over the Pd/CZHP-a and Pd/CZM-a catalysts. The results suggest that, compared with CZHP and CZM, more strong interaction exists between Pd species and CZCP or CZH after aging, which is in good agreement with XPS results.

In summary, it suggests that, for their practical application, the $Ce_{0.67}Zr_{0.33}O_2$ aged samples prepared by the microemulsion and homogeneous precipitation do not seem to be in a better position as support in view of reducibility.

3.6. OSCC measurements

OSCC values of $Ce_{0.67}Zr_{0.33}O_2$ samples measured at 400 °C are shown in Fig. 10. For the fresh samples, their O_2-uptake order is as follows: CZM > CZH > CZCP > CZHP, which is in good agreement with Raman results. The sample prepared by microemulsion displays the best OSCC among the fresh $Ce_{0.67}Zr_{0.33}O_2$ samples. For the aged samples, the OSCC is decreased and the value is 330.9, 134.7, 360.1 and 128.4 μmol/g for CZCP, CZHP, CZH and CZM, respectively. The CZM shows severe degradation of the OSCC value from 579.6 μmol/g to 128.4 μmol/g after aging, which indicates that the sample prepared by microemulsion exhibits the worst thermal stability. However, the samples prepared from hydrothermal and coprecipitation retain much higher OSCC than those prepared by homogeneous precipitation and microemulsion even after aging. These results indicate that the OSCC values can be strongly enhanced by increasing the homogeneity and defect of the solid solution. For example, at 400 °C, the OSCC values are 579.6 and 405.0 μmol/g for fresh CZM and CZH, but for the fresh CZCP sample the value is 388.7 μmol/g. Especially, the OSCC value drops to 159.8 μmol/g for fresh CZHP sample which exhibits the most heterogeneous property. Moreover, based on our measurements, it is suggested that the aging of the $Ce_{0.67}Zr_{0.33}O_2$ samples causes a loss of oxygen storage capacity due to sintering and segregation of Ce- and Zr-rich phases.

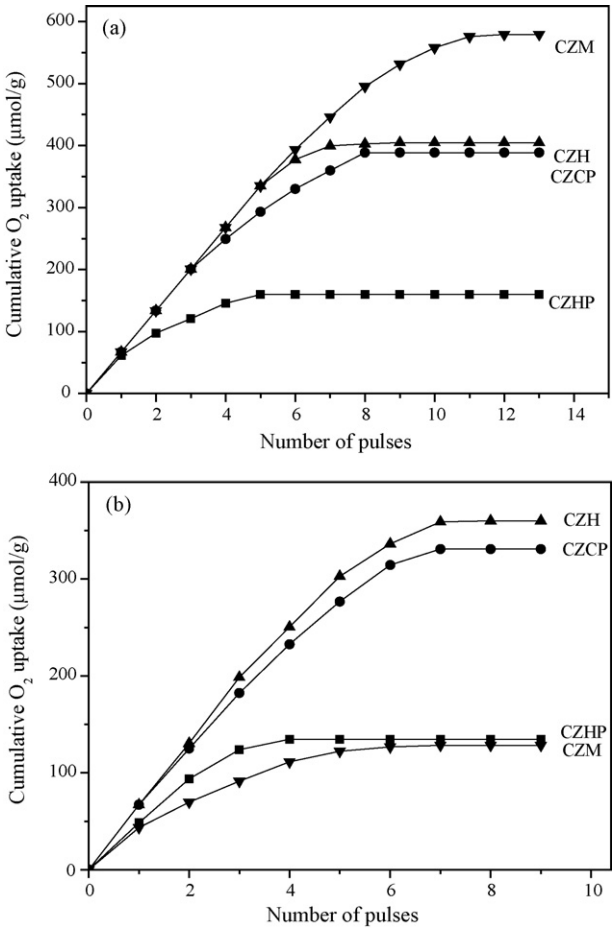

Fig. 11. Cumulative evolution of the O_2 uptake during the pulses experiments carried out at 400 °C over the (a) fresh and (b) aged $Ce_{0.67}Zr_{0.33}O_2$ samples prepared by different methods.

3.7. Kinetic aspects of the OSCC

Differences between the samples are also observed in the kinetics of oxidation at 400 °C. The results expressed as cumulative O_2 uptake versus the number of pulses are presented in Fig. 11. It demonstrates that the kinetics of the O_2 uptake is significantly affected by the preparation method and treatment process of the samples. Fig. 11(a) shows that the CZM and CZH samples exhibit a linear type of O_2 uptake for the first five pulses, which suggests that the initial response of these samples is fast. However, these two samples show a decreased O_2 uptake after the sixth pulse,

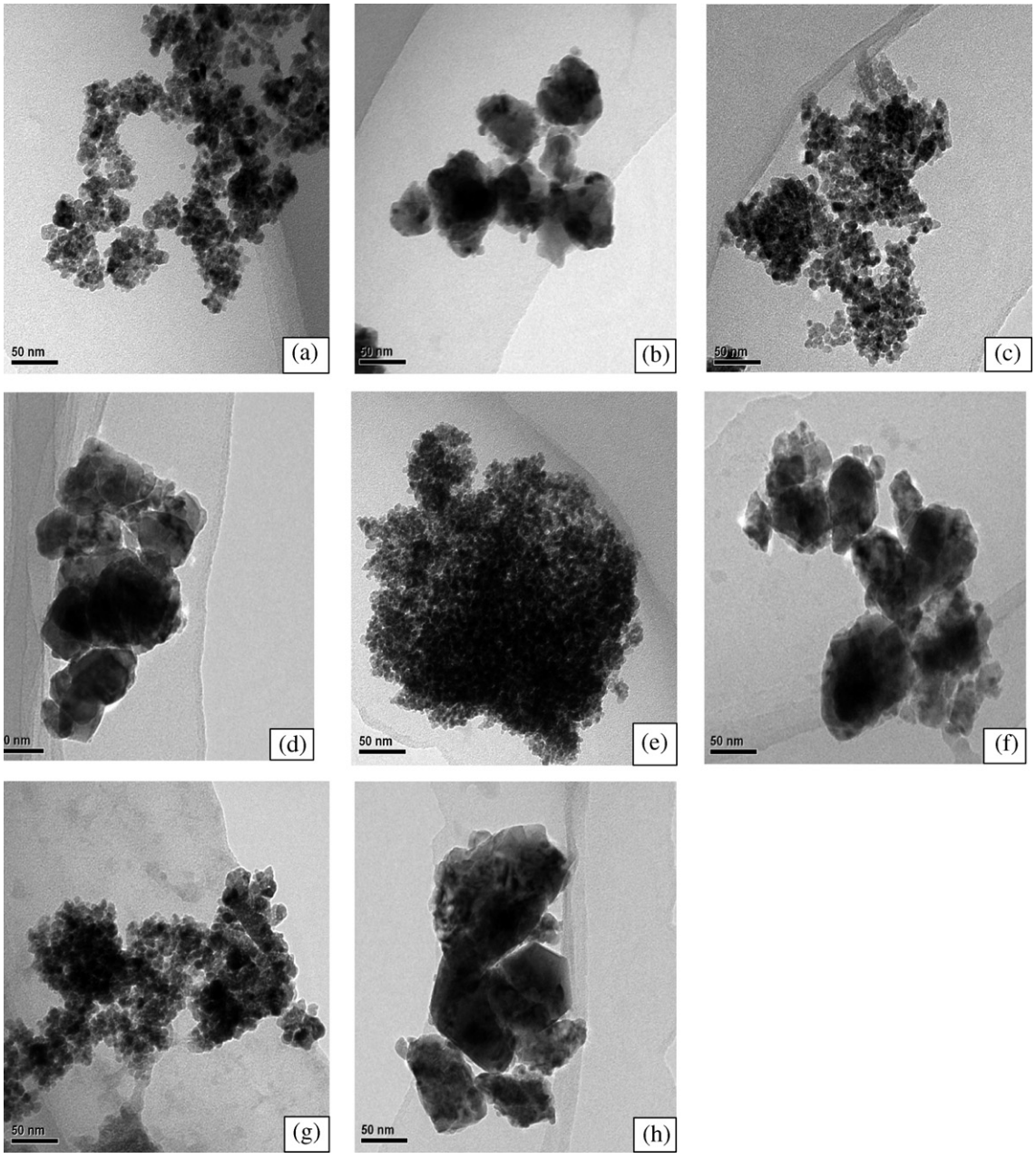

Fig. 12. The TEM photograph of the catalysts: (a) Pd/CZCP; (b) Pd/CZCP-a; (c) Pd/CZH; (d) Pd/CZH-a; (e) Pd/CZM; (f) Pd/CZM-a; (g) Pd/CZHP; (h) Pd/CZHP-a.

indicating that the kinetics of the O_2 uptake is slower until the full reoxidation are achieved. The kinetics of the O_2 uptake of the fresh samples follows the sequence of CZM > CZH > CZCP > CZHP, which is in accordance with the results obtained in Section 3.6. The kinetics of the O_2 uptake is deteriorated after aging treatment of the samples and that of the aged samples follows the sequence of CZH > CZCP > CZHP > CZM. According to Madier et al. [67], a $Ce_{0.68}Zr_{0.32}O_2$ solid solution has a theoretical OSC of 3.8 μmol "O" m^{-2} assuming that there is no surface segregation of the Ce^{4+} and Zr^{4+} cations and an equal distribution of the (1 0 0), (1 1 0), and (1 1 1) planes. Meanwhile, it is noted that the theoretical number of surface oxygen atoms (atoms-O nm^{-2}) differ by no more than 1.5% in the case of $Ce_xZr_{1-x}O_2$ ($x > 0.5$) in either cubic or tetragonal crystal structures. It allows us take the same value of 3.8 μmol "O" m^{-2} for our CZ mixed oxides of a similar composition. Hereby, the theoretical OSC supplied by monolayer of surface aged mixed oxides is 10.3, 5.9, 13.7 and 4.9 μmol O_2/g for CZCP, CZHP, CZH and CZM, respectively, which is far below the OSCC values of corresponding aged $Ce_{0.67}Zr_{0.33}O_2$ samples. Then it can be deduced that great mobility and diffusion effects of bulk oxygen exist for the aged $Ce_{0.67}Zr_{0.33}O_2$ samples, as already shown in the literature [68]. In addition, it should be noticed that the kinetics of the O_2 uptake of the aged CZM sample is remarkably slower than that of the fresh sample. However, the aged CZH and CZCP samples show much faster kinetics than CZM and CZHP.

In summary, the results of the investigation of redox properties clearly show that aging treatment modifies the properties of the $Ce_{0.67}Zr_{0.33}O_2$ samples, especially for the samples prepared by homogeneous precipitation and microemulsion methods.

3.8. TEM characterization of the catalysts

Fig. 12 gives the TEM pictures of different catalysts calcined at 500 and 1100 °C. The average particle sizes are 8.11, 9.43, 10.98 and

13.65 nm for Pd/CZM, Pd/CZH, Pd/CZCP and Pd/CZHP, respectively. After aging, the sintering of PdO and support occurs obviously, and the average particle sizes increase to 54.85, 46.44, 44.70 and 85.43 nm for Pd/CZM-a, Pd/CZH-a, Pd/CZCP-a and Pd/CZHP-a, respectively. This is due to the higher pretreatment temperature leading to a decrease in surface area, which causes poor dispersion of PdO and support. But for Pd/CZM and Pd/CZHP catalysts, the changes of the particle size are more obvious before/after calcined at 1100 °C compared to those of Pd/CZCP and Pd/CZH catalysts. This indicates that the CeO_2-ZrO_2 mixed oxides prepared by coprecipitation and hydrothermal can improve the thermal stability of the supported Pd catalysts because of the increase in the thermal stability of supports together with the strong interaction between Pd species and the supports, as already shown by XPS and TPR results.

3.9. The stoichiometric windows performance

The results of air/fuel (S) over fresh catalysts are shown in Fig. 13. The left side of the theoretical stoichiometric value ($S = 1$) is lean oxygen, and the right is rich oxygen. For fresh catalyst, it can be observed that the conversion of CO on all samples reaches 100% under $S \geq 1$ conditions. However, the conversion of CO descends with decreasing S value under $S < 1$ conditions. Pd/CZHP, Pd/CZH and Pd/CZM show almost the same oxidation activity for CO and Pd/CZCP exhibits slightly higher activity for CO than Pd/CZHP, Pd/CZH and Pd/CZM. With regard to HC conversion, the preparation method has a pronounced effect in the whole S-value range investigated. The order of catalytic activity for HC oxidation is Pd/CZCP > Pd/CZHP ≈ Pd/CZH > Pd/CZM and the conversion of HC descends with decreasing S value under $S < 1$ conditions. Wang et al. [66] have reported that in the case of Pd/CZ catalyst, PdO is reduced to Pd^0 under lean oxygen condition, which results in the decrease of the catalytic activity for HC oxidation. The same phenomenon has also been observed by Maillet et al. [69]. Furthermore, From Fig. 13 it is worth noting that the HC conversion remains 100% on Pd/CZCP and Pd/CZHP samples under $S > 1$ conditions but the oscillation can be observed over Pd/CZH and Pd/CZM catalysts, which may be related to the reaction mechanism and further studies need to be carried out to elucidate this point. The NO_x ($NO + NO_2$) conversion reaches 100% under $S \leq 1$ conditions but decreases obviously with increasing S-value under $S > 1$ conditions. The Pd/CZCP sample also shows the highest conversion of NO_x in the whole range.

In the case of aged catalysts, the Pd/CZCP-a catalyst shows wider amplitude of stoichiometric window than others. As shown in Fig. 14, it displays a higher activity for CO and HC conversion than other samples under $S < 1$ conditions. With regard to CO conversion, the differences in activities are slight among all these catalysts. But for the HC oxidation, the differences become obvious. The catalytic activities for HC oxidation follows the sequence of Pd/CZCP-a > Pd/CZH-a > Pd/CZHP-a > Pd/CZM-a under $S < 1$ conditions. Moreover, the HC conversions on all aged catalysts are decreased compared with fresh catalysts due to the sintering. As for the NO_x conversion, the aged Pd/CZM catalyst exhibits the worst activity and NO_x could be completely converted only at the point of $S = 0.8$.

CO, HC and NO_x conversions at different S (0.80, 1.00, and 1.12, respectively) values are shown in Table 3. S value width (W) acts as another scale to evaluate catalyst property when CO, HC and NO_x conversions all reach to 80% under rich and lean conditions. For example, the upper limit of the stoichiometric windows is limited by NO_x conversion under rich condition; the lower limit is limited by CO conversion under lean conditions for all samples. The upper limit subtracts the lower limit of S is W value. Furthermore, the wider the W value is, the broader the three-way working window is. The data in Table 3 indicate that for the fresh catalyst, at the stoichiometric ratio of the reaction mixture ($S = 1$), CO, HC and

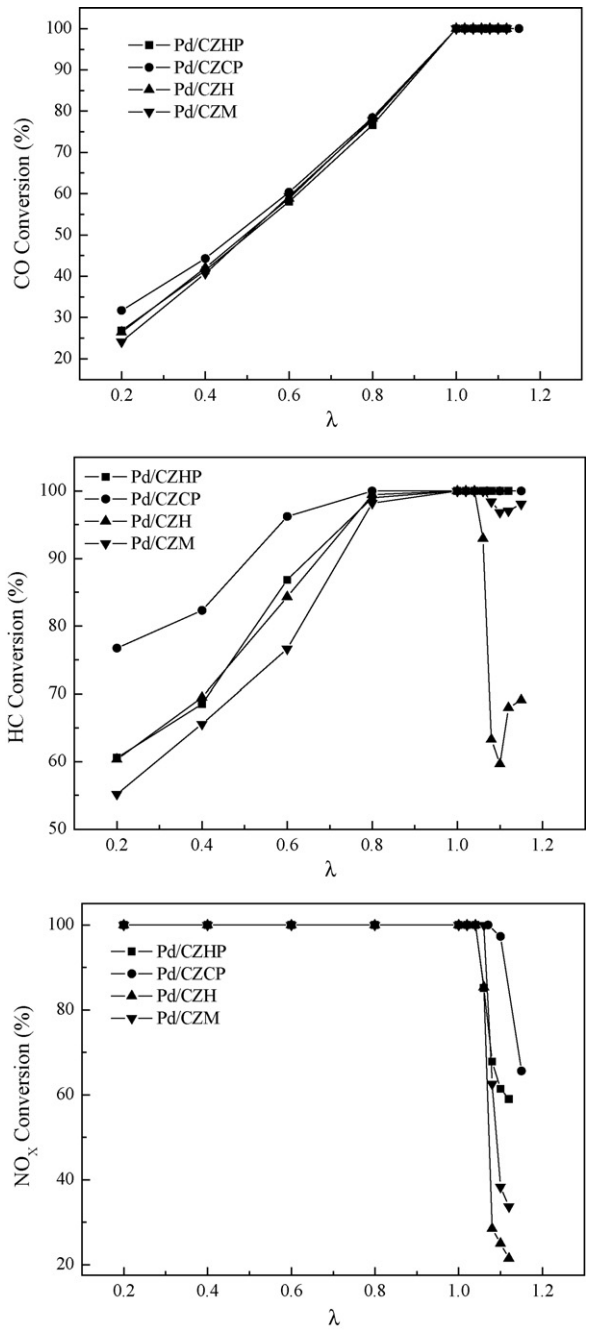

Fig. 13. Conversion curves of HC, CO and NO_x as a function of air/fuel ratio over fresh catalysts based on different supports.

NO_x are all completely converted and the activity is not related to the preparation method of the support. Moreover, at $S = 0.8$, fresh catalysts have similar activity for CO, HC and NO_x conversion but the differences in HC and NO_x conversion become obvious at $S = 1.12$. The Pd/CZCP catalyst exhibits the widest working window due to having the biggest W value (the sequence of the W value is Pd/CZCP > Pd/CZM > Pd/CZH = Pd/CZHP). For aged catalysts, the differences in the reactants conversion become more obvious compared with fresh catalysts and the W value follows the sequence of Pd/CZCP-a > Pd/CZH-a > Pd/CZHP-a ≫ Pd/CZM-a (exhibits no window). Based on the above analysis, we know that fresh Pd/CZCP catalyst exhibits the best reduction capacity, which is favorable for high catalytic activity. On the other hand, the pore-size distribution of support seems to be more important for fresh catalyst.

Table 3
CO, HC, NO_x conversion (%) of catalysts at different *S* values.

Catalyst	Conversion (%)									*W*
	S = 0.8			*S* = 1.0			*S* = 1.12			
	CO	HC	NO_x	CO	HC	NO_x	CO	HC	NO_x	
Pd/CZCP	78	100	100	100	100	100	100	100	84	0.32
Pd/CZHP	77	99	100	100	100	100	100	100	59	0.24
Pd/CZH	78	99	100	100	100	100	100	68	21	0.24
Pd/CZM	78	98	100	100	100	100	100	97	34	0.25
Pd/CZCP-a	81	98	100	100	100	100	100	98	64	0.28
Pd/CZHP-a	78	79	100	97	100	100	100	84	58	0.22
Pd/CZH-a	79	91	100	99	100	100	100	94	60	0.27
Pd/CZM-a	81	43	100	100	80	76	100	71	40	–

W: width of *S* values when CO, HC and NO_x conversions all reach to 80% under rich or lean conditions.

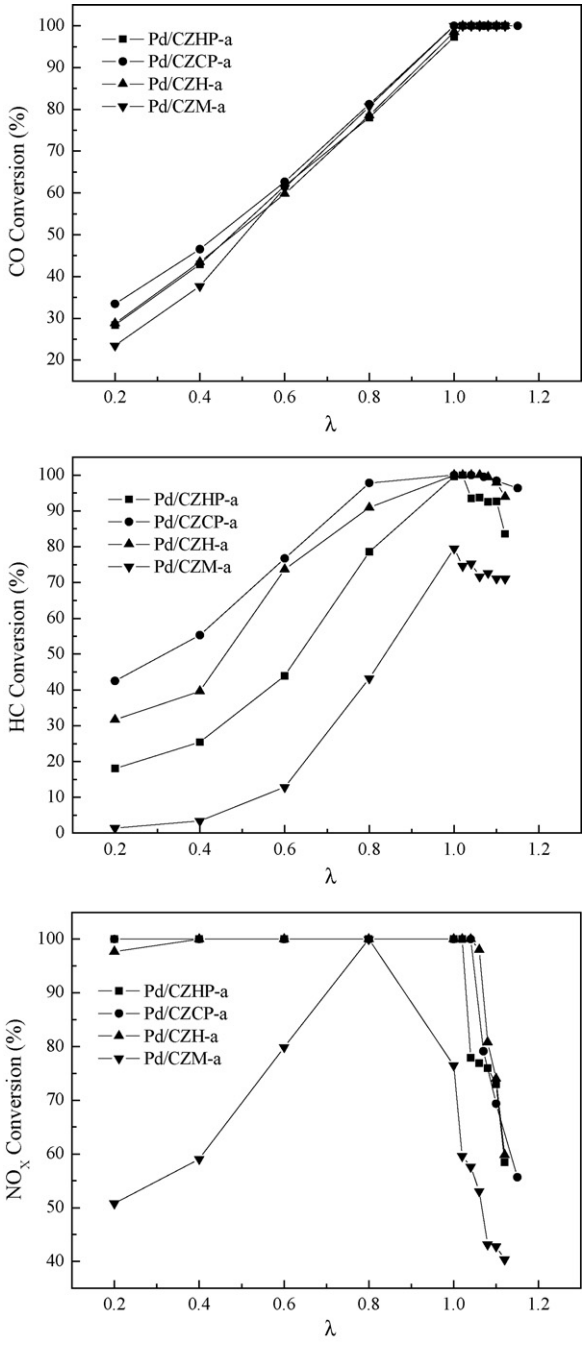

Fig. 14. Conversion curves of HC, CO and NO_x as a function of air/fuel ratio over aged catalysts based on different supports.

For example, the pore distribution is uniform for fresh CZCP and the maximum of pore distribution is observed at around 20.87 nm, which is obviously larger than others. In addition, the mesopore volume of fresh CZCP is also the largest (0.455 cm^3/g). So CZCP sample as the catalytic support employed in high space velocity condition shows the best catalytic activity [70,71]. For aged catalysts, their activities are related to both the redox properties and the textural properties of aged mixed oxides. For example, for the aged CZM, the surface area is found to decrease drastically and the value is only 2.6 m^2/g. As a result, Pd/CZM-a exhibits no stoichiometric window due to the serious sintering of support together with the deterioration of support redox property. Contrarily, aged CZH and CZCP have larger surface areas and better redox properties than aged CZHP and CZM. Consequently, Pd/CZCP-a and Pd/CZH-a catalysts still exhibit higher catalytic activities. In summary, CZCP used as support amplifies the amplitude of stoichiometric window for the fresh and aged catalyst. Three factors may be considered mainly responsible for this consequence: first, fresh sample prepared by the special drying method (supercritical condition in alcohol) contains suitable pore distribution which is favorable for high catalytic activity in high space velocity condition; second, the better OSCC value and the formation of oxygen vacancies can have consequences on the superior reactivity toward NO_x; third, the CZCP sample possesses good redox property before and after aging and good textural stability.

4. Conclusions

The textural and structural properties as well as the redox behaviors of the $Ce_{0.67}Zr_{0.33}O_2$ mixed oxides strongly depend on the preparation routes. For example, more homogeneously nanodispersed $Ce_{0.67}Zr_{0.33}O_2$ sample is successfully obtained by microemulsion, leading to a maximal O_2 uptake in the OSCC analysis and favorable reducibility behavior in the TPR analysis. After calcinations at 1100 °C for 4 h, however, it experiences severe sintering and hereby the reduction peaks of surface oxygen species disappear. The aged CZM sample shows the worst properties of both OSCC values and the kinetics of the O_2 uptake among the aged samples. As far as the homogeneous precipitation method is concerned, the heterogeneity and sintering severely affect the redox properties. On the contrary, the aged samples prepared by the coprecipitation and hydrothermal methods keep low-temperature reducibility and preferable oxygen storage capacity. The results of the activity tests show that the pore-size distribution of mixed oxides seems to be important for the fresh catalyst. In addition, catalytic activity is related to both the redox properties and the textural properties of aged mixed oxides. Consequently, CZCP as support amplifies the amplitude of stoichiometric window for the fresh and aged catalyst. Three factors may be considered mainly responsible for this consequence: first, fresh sample prepared by the special drying method (supercritical condition in alcohol) has

suitable pore distribution which is favorable for high catalytic activity in high space velocity condition; second, the better OSCC value and the formation of oxygen vacancies can have consequences on the superior reactivity toward NO_x; third, the CZCP sample possesses good redox property before and after aging and good textural stability.

In addition, one of the biggest issues for three-way catalysts is the degradation of catalytic activity caused by sintering. To achieve a good balance between catalytic activity and the sintering suppression, it is found that doping a proper third component as a stabilizer to $Ce_xZr_{1-x}O_2$ solid solutions (CZM) can improve the ceria–zirconia thermal resistance. Further investigations would be necessary to ascertain the proper preparation method for CZM mixed oxide supports.

Acknowledgement

We gratefully acknowledge the financial supports from the Ministry of Science and Technology of China (Nos. 2006AA060306, 2009AA064804).

References

[1] X. Liang, X. Wang, Y. Zhuang, B. Xu, S.M. Kuang, Y.D. Li, J. Am. Chem. Soc. 130 (2008) 2736–2737.
[2] S. Damyanova, B. Pawelec, K. Arishtirova, M.V. Martinez Huerta, J.L.G. Fierro, Appl. Catal. A 337 (2008) 86–96.
[3] P.F. Ji, J.L. Zhang, F. Chen, M. Anpo, Appl. Catal. B 85 (2009) 148–154.
[4] B. de Rivas, R. López-Fonseca, C. Sampedro, J.I. Gutiérrez-Ortiz, Appl. Catal. B 90 (2009) 545–555.
[5] Y. Denkwitz, A. Karpenko, V. Pizak, R. Leppelt, B. Schumacher, R.J. Behm, J. Catal. 246 (2007) 74–90.
[6] A. Pintar, J. Batista, S. Hočevar, J. Colloid Interface Sci. 307 (2007) 145–157.
[7] M. Boaro, M. Vicario, J. Llorca, C. De Leitenburg, G. Dolcetti, A. Trovarelli, Appl. Catal. B 88 (2009) 272–282.
[8] B.M. Reddy, P. harali, P. aikia, J. Phys. Chem. C 112 (2008) 11729–11737.
[9] F. Mariño, C. Descorme, D. Duprez, Appl. Catal. B 58 (2005) 175–183.
[10] A. Papavasiliou, A. Tsetsekou, V. Matsouka, M. Konsolakis, I.V. Yentekakis, N. Boukos, Appl. Catal. B 90 (2009) 162–174.
[11] M.Q. Shen, M. Yang, J. Wang, J. Wen, M.W. Zhao, W.L. Wang, J. Phys. Chem. C 113 (2009) 3212–3221.
[12] X.D. Wu, J. Fan, R. Ran, J. Yang, D. Weng, J. Alloys Compd. 395 (2005) 135–140.
[13] B.M. Reddy, P. Lakshmanan, A. Khan, C.L. Cartes, T.C. Rojas, A. Fernandez, J. Phys. Chem. B 109 (2005) 1781–1787.
[14] M.P. Yeste, J.C. Hernández, S. Bernal, G. Blanco, J.J. Calvino, J.A. Pérez-Omil, J.M. Pintado, Chem. Mater. 18 (2006) 2750–2757.
[15] E.V. Kondratenko, Y. Sakamoto, K. Okumura, H. Shinjoh, Appl. Catal. B 89 (2009) 476–483.
[16] H. Vidal, S. Bernal, J. Kašpar, M. Pijolat, V. Perrichon, G. Blanco, J.M. Pintado, R.T. Baker, G. Colon, F. Fally, Catal. Today 54 (1999) 93–100.
[17] F. Fally, V. Perrichon, H. Vidal, J. Kašpar, G. Blanco, J.M. Pintado, S. Bernal, G. Colon, M. Daturi, J.C. Lavalley, Catal. Today 59 (2000) 373–386.
[18] A. Morikawa, K. Kikuta, A. Suda, H. Shinjo, Appl. Catal. B 88 (2009) 542–549.
[19] X.D. Wu, B. Yang, D. Weng, J. Alloys Compd. 376 (2004) 241–245.
[20] H.Q. Wan, D. Li, H.Y. Zhu, Y.H. Zhang, L.H. Dong, Y.H. Hu, B. Liu, K.Q. Sun, L. Dong, Y. Chen, J. Colloid Interface Sci. 326 (2008) 28–34.
[21] R. Di Monte, J. Kašpar, J. Mater. Chem. 15 (2005) 633–648.
[22] H.S. Potdar, S.B. Deshpande, A.S. Deshpande, S.P. Gokhale, S.K. Date, Y.B. Khollam, A.J. Patil, Mater. Chem. Phys. 74 (2002) 306–312.
[23] Z.L. Zhang, Y.X. Zhang, Z.G. Mu, P.F. Yu, X.Z. Ni, S.L. Wang, L.S. Zheng, Appl. Catal. B 76 (2007) 335–347.
[24] A.E. Nelson, K.H. Schulz, Appl. Surf. Sci. 210 (2003) 206–221.
[25] T. Luo, R.J. Gorte, Appl. Catal. B 53 (2004) 77–85.
[26] V. Raju, S. Jaenicke, G.K. Chuah, Appl. Catal. B 91 (2009) 92–100.
[27] S. Letichevsky, C.A. Tellez, R.R. de Avillez, M.I.P. da Silva, M.A. Fraga, L.G. Appel, Appl. Catal. B 58 (2005) 203–210.
[28] A. Cabañas, J.A. Darr, E. Lester, M. Poliakoff, J. Mater. Chem. 11 (2001) 561–568.
[29] M. Yashima, K. Ohtake, M. Kakihana, M. Yoshimura, J. Am. Ceram. Soc. 77 (1994) 2773–2776.
[30] M.F. Luo, G.L. Lu, X.M. Zheng, Y.L. Zhong, T.H. Wu, J. Mater. Sci. Lett. 17 (1998) 1553–1557.
[31] M. Thammachart, V. Meeyoo, T. Risksomboon, S. Osuwan, Catal. Today 68 (2001) 53–61.
[32] H.S. Potdar, S.B. Deshpande, Y.B. Khollam, A.S. Deshpande, S.K. Date, Mater. Lett. 57 (2003) 1066–1071.
[33] N. Laosiripojana, S. Assabumrungrat, Appl. Catal. B 60 (2005) 107–116.
[34] M.Q. Shen, J.Q. Wang, J.C. Shang, Y. An, J. Wang, W.L. Wang, J. Phys. Chem. C 113 (2009) 1543–1551.
[35] W.J. Stark, L. Mädler, M. Maciejewski, S.E. Pratsinis, A. Baiker, Chem. Commun. 3 (2003) 588–589.
[36] A. Cabanas, J.A. Darr, M. Poliakoff, E. Lester, Chem. Commun. 0 (2000) 901–902.
[37] D.G. Lamas, R.O. Fuentes, I.O. Fábregas, M.E.F. de Rapp, G.E. Lascalea, J.R. Casanova, N.E.W. de Reca, A.F. Craievich, J. Appl. Crystallogr. 38 (2005) 867–873.
[38] M. Alifanti, B. Baps, N. Blangenois, J. Naud, P. Grange, B. Delmon, Chem. Mater. 15 (2003) 395–403.
[39] C.E. Hori, H. Permana, K.Y. Simon Ng, A. Brenner, K. More, K.M. Rahmoeller, D. Belton, Appl. Catal. B 16 (1998) 105–117.
[40] D. Terribile, A. Trovarelli, J. Llorca, C. de Leitenburg, G. Dolcetti, Catal. Today 43 (1998) 79–88.
[41] Y. Li, Q. Fu, M.F. Stephanopoulos, Appl. Catal. B 27 (2000) 179–191.
[42] H. He, M. Liu, H.X. Dai, W.G. Qiu, X.H. Zi, Catal. Today 126 (2007) 290–295.
[43] S. Nassos, E.E. Svensson, M. Nilsson, M. Boutonnet, S. Jaras, Appl. Catal. B 64 (2006) 96–102.
[44] P.F. Zhu, J. Li, S.F. Zuo, R.X. Zhou, Appl. Surf. Sci. 255 (2008) 2903–2909.
[45] J. Kašpar, P. Fornasiero, N. Hickey, Catal. Today 77 (2003) 419–449.
[46] J.R.G. Velasco, J.A. Botas, J.A.G. Marcos, M.A.G. Ortiz, Appl. Catal. B 12 (1997) 61–79.
[47] Y. Qi, S. Qiu, Z.G. Zhang, Y. Guo, G.Z. Lu, Y.L. Guo, J. Chin. Rare Earth Soc. 23 (2005) 51–54.
[48] T. Masui, K. Fujiwara, Y. Peng, T. Sakata, K.I. Machida, H. Mori, G.Y. Adachi, J. Alloy Compd. 269 (1998) 116–122.
[49] K. Kenevey, F. Valdivieso, M. Soustelle, M. Pijolat, Appl. Catal. B 29 (2001) 93–101.
[50] X.D. Wu, X.D. Wu, Q. Liang, J. Fan, D. Weng, Z. Xie, S.Q. Wei, Solid State Sci. 9 (2007) 636–643.
[51] I. Atribak, A.B. López, A.G. Carcía, J. Mol. Catal. A 300 (2009) 103–110.
[52] P. Singh, M.S. Hegde, Chem. Mater. 21 (2009) 3337–3345.
[53] J. Fan, X.D. Wu, X.D. Wu, Q. Liang, R. Ran, D. Weng, Appl. Catal. B 81 (2008) 38–48.
[54] J. Fan, D. Weng, X.D. Wu, X.D. Wu, R. Ran, J. Catal. 258 (2008) 177–186.
[55] H.W. Jen, G.W. Graham, W. Chun, R.W. McCabe, J.P. Cuif, S.E. Deutsch, O. Touret, Catal. Today 50 (1999) 309–328.
[56] D.H. Kim, S.I. Woo, J. Noh, O.B. Yang, Appl. Catal. A 207 (2001) 69–77.
[57] X.D. Wu, J. Fan, R. Ran, D. Weng, Chem. Eng. J. 109 (2005) 133–139.
[58] S. Pengpanich, V. Meeyoo, T. Rirksomboon, K. Bunyakiat, Appl. Catal. A 234 (2002) 221–233.
[59] R. Si, Y.W. Zhang, S.J. Li, B.X. Lin, C.H. Yan, J. Phys. Chem. B 108 (2004) 12481–12488.
[60] T. Masui, K. Nakano, T. Ozaki, G. Adachi, Z. Kang, L. Eyring, Chem. Mater. 13 (2001) 1834–1840.
[61] B.M. Reddy, A. Khan, Langmuir 19 (2003) 3025–3030.
[62] W.J. Shan, Z.C. Feng, Z.L. Li, J. Zhang, W.J. Shen, C. Li, J. Catal. 228 (2004) 206–217.
[63] Z.L. Wei, H.M. Li, X.Y. Zhang, S.H. Yan, Z. Lv, Y.Q. Chen, M.C. Gong, J. Alloys Compd. 455 (2008) 322–326.
[64] J.R. Kim, W.J. Myeong, S.K. Ihm, Appl. Catal. B 71 (2007) 57–63.
[65] B.H. Yue, R.X. Zhou, Y.J. Wang, X.M. Zheng, Appl. Catal. A 295 (2005) 31–39.
[66] J.Q. Wang, M.Q. Shen, Y. An, J. Wang, Catal. Commun. 10 (2008) 103–107.
[67] Y. Madier, C. Descorme, A.M. Le Govic, D. Duprez, J. Phys. Chem. B 103 (1999) 10999–11006.
[68] S. Salasc, V. Perrichon, M. Primet, N. Mouaddib-Moral, J. Catal. 206 (2002) 82–90.
[69] T. Maillet, C. Solleau, J. Barbier Jr., D. Duprez, Appl. Catal. B 14 (1997) 85–95.
[70] J. Noh, O.B. Yang, D.H. Kim, S.I. Woo, Catal. Today 53 (1999) 575–582.
[71] D.H. Kim, S.I. Woo, O.B. Yang, Appl. Catal. B 26 (2000) 285–289.